Skin structure of the slow worm lizard Anguis fragilis (Anguidae, Sauria, Reptilia) with emphasis on the epidermal micro-ornamentation in relation to the animal movements

Skin structure of the slow worm lizard *Anguis fragilis* (Anguidae, Sauria, Reptilia) with emphasis on the epidermal micro-ornamentation in relation to the animal movements

Antonio Bonfitto*, Maria Roberta Randi*, Lorenzo Alibardi*°

*Department of Biology, BIGEA, University of Bologna, Italy

°Comparative Histolab Padova

Correspondence: L. Alibardi, BIGEA, via Selmi 3. 40126, Bologna, Italy

Runninghead: microornamentation in the slow worm lizard

Abstract

Skin structure of the slow worm lizard *Anguis fragilis* (Anguidae, Sauria, Reptilia) with emphasis on the epidermal micro-ornamentation in relation to the animal movements (Acta Zoologica, Stockolm)

The structure of the skin and superficial micro-ornamentation in the slow worm *Anguis fragilis*, a limbless lizard with a fossorial activity, was examined using histology, immunofluorescence, scanning and transmission electron microscopy. The scales, with a triangular to trapezoidal shape, are very overlapped and interlocked to form a smooth surface, and are reinforced by osteoderms. The epidermis shows a thin Oberhautchen layer merged with a thicker beta-layer than contain corneous beta-proteins. The SEM survey detects a smooth surface made by tile-like patterned Oberhautchen cells with irregular perimeters that form an interlocking surface. Disk-like sensory organs of 15-20 μm diameter are observed only on the head scales, the first to sense the environment and contact the ground. Numerous Oberhautchen denticles, namely corneous thorns of about 0.2-0.3 μm, adorn the caudally directed perimeter of Oberthautchen cells in the ventral scales of the trunk and tail. This microstructure may determine gripping and increased friction with the substrate during the lateral undulating and forward movements of the slow worm. TEM observations reveal sparse short serrated protrusions of Oberhautchen cells that are largely merged with the underlying beta-cells. Altogether the scale surface of the slow worm efficiently suites this limbless lizard to its environment and lifestyle.

Keywords: lizard; skin; SEM; TEM; immunolabeling

1. INTRODUCTION

Among lizard families, those with reduction of limb size or even complete lack of anterior, posterior or even both limbs comprise the scincid and anguid families (Pough et al., 2001). The reduction or even the loss of limbs in lizards determines the acquisition of a serpentiform modality of locomotion united to the specialization of the skin surface toward a "streamline terrestrial adaptation" that allows the undulatory movement and also facilitates the penetration in the soil and, in some species, even underground movements in sandy environment such as deserts (Staudt et al., 2012; Spinner et al., 2015; Canei and Nonclercq, 2021).

The European slow worm (or blindworm) *Anguis fragilis*, belonging to the Family Anguidae, is a serpentiform-shaped and legless lizard adapted to slither both in open spaces such as grasslands, among rocky areas, and is also capable of a fossorial life (Shortridge, 2023). Its shiny skin appears compact and solidly attached to the underlying muscles and gives rise to a stiff skin surface that allows strong lateral movements during forward-backward progression. Like many scincids, also anguids possess extremely overlapped scales, a pattern that likely represents an adaptation to their serpentiform movement and fossorial activity and that maintains compact and "streamline in a terrestrial environment" ("sand-swimming") their surface, facilitating a rapid digging and borrowing. Aside the epidermis, the dermis of numerous scincids and anguids presents a dermal reinforcement derived from the formation of extended osteoderms (Zylberberg and Castanet, 1985;Vickaryous and Sire, 2009; Williams et al., 2022; Cherepanov et al., 2023).

Since the epidermis and its asperities are the contact surface with the ground for the serpentiform movement, it would be important to determine the microscopic details of the skin surface and consequently of the external, hard corneous layer. The latter is subjected to a high wear due to the abrasion determined by the slithering modality of movement. The external layer of lizards and snakes, termed Oberhautchen presents microsculptures of different types, and is likely the main tissue subjected to various degree of wearing. The corneous layer is frequently shed and, since the initial development of the skin, consists in an external Oberhautchen-beta-layer and an internal alpha-layer (Maderson et al., 1998; Alibardi, 1999, 2014a,b; Alibardi and Toni, 2006; Swadzba and Rupik, 2010). During formation of the successive epidermal layers in the renewal phase of the cyclical shedding cycle of lizards and snakes, a superficial layer called Oberhautchen is originated from the basal layer of the epidermis, and forms a microsculpture or micro-ornamentation characteristics for different species (Ruibal, 1968; Stewart and Daniels, 1973; Price, 1982; Smith et al., 1982; Irish et al., 1988; Price and Kelly, 1989; Alibardi, 1999; Rhoca-Barbosa and e Silva, 2009; Dujsebayeva et al., 2021). The single Oberhautchen layer matures and merges with the 3-6

layers of beta-cells produced underneath giving rise to a compact Oberhautchen-beta-layer with a main role for the mechanical protection of the epidermis. Osteoderms also contribute to the mechanical protection of the dermis and underlying softer tissues. The present study provides some microscopic details on the un-described general structure of the skin in this species, the slow worm, with emphasis on the more superficial corneous layers, involved in the serpentine movement of this animal.

2. MATERIALS AND METHODS

The samples derived from three juvenile individuals of slow worm (*Anguis fragilis*, Linnaeus, 1758), likely recently killed by cats. In two animals of about 15 cm in length, pieces of 3-5 mm of the trunk skin were immediately fixed in 5% neutral formaldehyde for 1 day, and skin samples were dehydrated and embedded in Bioacryl resin under UV at 0-4°C (Scala et al., 1992). The remaining specimen of about 7.5 cm in length was fixed (whole) for about 2 days in neutral formaldehyde 10%, rinsed in distilled water for few minutes and stored in 70% ethanol.

The resin-embedded samples from the two specimens were sectioned using an ultramicrotome at 2-4 μm thickness (semithin sections), and the sections were attached to glass slides pre-coated with gelatine-chromoallume for the following histological and immunohistochemical study. For routine histology 0.5% toluidine blue was utilized. Other sections went through the von Kossa reaction for revealing calcium phosphate (Mazzi, 1977). Other semithin sections were instead utilized for immunofluorescence after application of rabbit primary antibodies against CBPs (Corneous Beta Proteins), such as the beta-1 and the pre-CB antibodies, as previously described (Alibardi and Toni, 2006; Alibardi, 2014a,b). The overnight incubation with the primary antibodies (dil 1: 100 in phosphate buffer with 2% BSA, Bovine Serum Albumin) at 0-4°C followed a pre-incubation of 1 h with 5% NGS (Normal Goat Serum) in neutral 0.1 M phosphate buffer with 2% BSA. In control sections the primary antibodies were omitted. After repeated rinsing in buffer, the sections were incubated for 70 minutes at room temperature with the anti-rabbit secondary antibodies (1: 200 dilution in buffer) conjugated with the fluorophores FITC (green) or TRITC (red). For nuclear counterstaining was utilized the blue fluorophore DAPI (1: 100 dilution in buffer). Some thin sections (50-100 nm thick) of the epidermis embedded in resin were also collected on 300 mesh copper grids, stained with uranyl acetate and lead citrate according to routine methods for the study under TEM (Transmission Electron Microscopy). The grids were analyzed under a 10 C/CR Zeiss

electron microscope operating at 60 kV and a Philips CM 100 electron microscope operating at 80 kV.

The third specimen went through SEM (Scanning Electron Microscope) preparation, for the study of the epidermal surface. On this purpose, after about 5 days of drying at room temperature, the body was subdivided in 6 pieces ranging in size from 10 mm (head) to 15-20 mm (trunk and tail), then the single pieces were immobilized on alluminium stubs of 5 mm in diameter that were previously coated with double-sticky tape for Scanning Electron Microscopic (SEM) analysis. The samples were double coated with gold using a metallizer device (BIO-RAD SEM Coating System, SC502), and observed at various magnifications under a SEM Hitachi S-2400 operating at 15 kV. Other observations at higher magnification have employed a "*Thermofisher Quattro S*" SEM powered by a field emission gun (FEG) for electron source.

3. RESULTS

3.1. Histology and Immunofluorescence

The slow worm is covered from very imbricated scales. The analyzed epidermis in the available samples showed a post-shedding condition (stage 1 of the shedding cycle) with 3-5 suprabasal and still immature alpha-layers located beneath the thick outer beta-layer (Fig. 1 A, B). The thick beta-layer, indicatively 4-8 μm thick, was so stiff and inflexible that often appeared detached partially or completely from the rest of the epidermis after sectioning. Large osteoderms were located in the superficial dermis, with their top layers of osteodermin (compact acellular bone) forming deep dome-like extensions that reached underneath the epidermis (Fig. 1 B). Most of the osteoderm was made of compact bone (not haversian) with various but sparse osteocytes. The von Kossa reaction indicated that the entire osteoderm contained calcium phosphate (Fig. 1 C).

Using antibodies for CBPs (beta-1 and preCB antibodies) the thick beta-layer of mature scales (Fig. 2 A) appeared immuno-fluorescent while the suprabasal layers of keratinocytes and forming alpha-cells remained immunonegative (Fig. 2 B-D). Also control sections (omitting the antibodies) were immunonegatives (Fig. 2 E).

3.2. Scanning electron microscopic observations

Cephalo-caudal regions of the animal analyzed were scanned for a general scale mapping in dorsal, lateral and ventral sides. The dorsal region of the head showed large scales of different shapes, polygonal to trapezoid, and variable sizes, and a very large nuchal scale was present (Fig. 3 A). The

surface of scales appeared quite smooth and the scales were tightly compacted, giving rise to a smooth external surface. In some regions of the head and trunk some scales featured little deformations or wore borders (arrows in Fig. 3 C, D) that may derive from an actual wearing process. The deformation or small detachments of the epidermal surface are likely artifactual alterations derived from the long ethanol storage and from the preparation of the specimen. On the more apical nasal and labial scales numerous circular bouton-shaped sensilli were observed (Fig. 3 B-D). They appeared as circular depressions of the epidermal surface formed by a tile-like pattern of Oberhautchen cells (Fig. 3 E, F). In these 15-20 μm large depressions, the thickness of Oberhautchen cells is therefore reduced in comparison to the remaining surface.

On the ventral side of the head (gular region) scales were larger and trapezoidal in the most apical region and smaller toward the base of the head and continuing in the trunk (Fig. 4 A). Also here sensilli were only detected in the more rostral scales of the jaw and also in labial scales (see later their mapped distribution). Like for the dorsal scales, sensilli appeared distributed along a curved line in the nasal, labial and ventral scales. Most scales were perfectly overlapped but their posterior-directed borders (perimeter) appeared damaged, likely wore (arrow in Fig. 4 B). Sensilli were absent in all the remaining body scales, in the trunk and tail.

The shape of most overlapped dorsal scales in the trunk, at least those of the exposed surface, was trapezoidal and their close imbrication gave rise to a smooth surface (Fig. 4 C). In the lateral sides of the trunk (flanks) the shape of very overlapped scales was rounded or the exposed scale surface featured a triangular shape (Fig. 4 D, E). Also here the perimeter of many scales appeared degraded or wore (arrows in Fig. 4 E). The observation at higher magnification of dorsal and flank scales showed a smooth surface composed by tile-patterned Oberhautchen cells with irregular perimeter (Fig. 4 F and inset).

The observations on the ventral scales of the trunk while revealing a similar trapezoidal shape as in the dorsal side also showed other details that were absent in the remaining body scales. Also in ventral scales the perimeter of numerous scales appeared wore or damaged (Fig. 5 A), and Oberhautchen cells formed a tile-like surface made of cells with a undulated or zig-zag irregular perimeter (Fig. 5 A, B). While Oberhautchen cells located in the central zone of scales featured similar length and a similar diameter in all directions (polygonal) cells approaching the scale border posteriorly tended to elongate in the lateral sides (more rectangular) turning much wider and orthogonal to the cephalo-caudal axis of the scale (Fig. 5 A-C). Apparently, the borders of some Oberhautchen cells were slightly overlapped with more posteriorly directed cells (Fig. 5 B, C). A peculiarity of more caudally located ventral scales was the elongated rectangular shape of Oberhautchen cells and the presence of a variable number of corneous denticles of about 0.2-0.3

μm along the posterior border. These microstructures were previously indicated as "echinated" in snakes (Price, 1982; Price and Kelly, 1989) or as "microridges" in lizards (Canei and Nonclercq, 2021; Fig. 5 C and inset).

Finally, also the tail region (located caudally to the cloacal fissure) showed similar general aspects as in the trunk, including the presence of microridges in the Oberhautchen cells of the ventral caudal scales (Fig. 6 A). Cell boundaries appeared sometimes slighly overlapped in caudal direction (inset in Fig. 6 A). Also numerous scales in the caudal region showed a perimeter with signs of wearing in the overlapped posterior margin of scales (arrows in Fig. 6 B).

3.3. Transmission electron microscopic observations

The study with the transmission electron microscope of mature caudal scales in post-shedding condition showed the typical layer sequence noted for other lizards. The thin fully cornified Oberhautchen in longitudinal section (cephalo-caudal) appeared slanted in both the outer and the inner scale surface (Fig. 6 C, D). These short protrusions (1-1.5 μm) correspond to the small overlapped borders of Oberhautchen cells as observed with SEM (inset in Fig. 6 A). In the outer scale surface (dorsal) the Oberhautchen was merged with the electron-paler beta-layer that contained a variable number of melanosomes, forming a relatively thick (5-10 μm) corneous layer (Fig. 6 C). The beta-layer thinned out toward the hinge region where it almost disappeared and was absent in the inner scale surface so that the serrated corneous surface here was only 1-2 μm thick (Fig. 6 D, E). Underneath the beta-layer of the outer scale surface, 3-5 layers of thin mesos cells were observed and they were more numerous in the hinge region and inner scale surface (Fig. 6 E).

An electron- dense corneous strip was located on the surface of the slanted Oberhautchen protrusion (Fig. 6 F). In both the denser Oberhautchen and in the paler beta-layer numerous sparse remnants of cell junctions derived from the fusion of cells into a sincytium were observed (Fig. 6 F, G). The fine granulation of the beta-layer presented variegated areas of electron-density indicating an heterogenous nature of the corneous material. The thin mesos-cells (0.2-0.5 μm thick) featured a granular intracellular and extracellular material, probably lipid or glycoplipidic in nature (Fig. 6 H).

4. DISCUSSION

4.1. General structure of the epidermis

The present study reveals that a thick beta-layer containing CBPs covers the scales of the slow worm, representing the first mechanical protection against the wearing activity of abrasion on the

epidermis derived from the movement, sliding, slithering activities of this reptile, like in snakes (Berthe et al., 2009; Klein and Gorb, 2014), further implemented from digging. The very overlapped scales directed posteriorly form an extremely compact and linear surface that is perfectly suited for slithering with the reduction of attrition, an activity that would be otherwise impossible to be carried out through tuberculate or simply slanted scales with little overlapping and exposing hinge regions. Extremely superimposed scales are typical of snakes and other limbless reptiles that crawl around by slithering. The TEM analysis has shown that the beta-layer is made by a slightly more electron dense rim of slanted Oberhautchen merged with a typical and electron-paler compact beta-layer, variably incorporating melanosomes. The study confirms that only an Oberhautchen but not a beta-layer is present in the inner side and hinge region of scales, like in other lizards and in snakes (Maderson et al., 1998; Alibardi and Toni, 2006; Swadza and Rupik, 2010). The available epidermis for this study only showed a post-shedding and resting stage with some typical mesos-layers formed underneath the epidermis and above the germinal layer.

The further mechanical skin protection and its compactness derive from the connective tissues that bridge the epidermis and the lowermost dermis with the underlying muscle fascia through highly calcified osteoderms, typical dermal reinforcements in numerous scincids and anguids (Zylberberg and Castanet, 1985; Vickaryous and Sire, 2009; Canei and Nonclercq, 2021; Williams et al., 2022; Cherepanov et al., 2023).

4.2. Microstructure of the epidermal surface

The pattern of microornamentation among lepidosaurians is very variable in different species, and is somehow associated with their specific environmental adaptation (Ruibal, 1968; Arnold, 2002; Gower, 2003; Rhoca-Barbosa and eSilva, 2009; Klein and Gorb, 2104). Numerous functions have been indicated for lepidosaurian microornamentation in different species, from regulating skin shedding, reflecting or diffracting solar light and creating visible colorations or iridescence, reflection for hiding from predators, antimicrobial or anti-parasite protection, blocking dust deposition and elimination of foulings, decrease or increase of friction, storing and dispersing pheromones and so forth. While in numerous anoline and gekkonid lizards microornamentation are dense and spinulated to favor friction and even adhesion through long bristles or setae (Maderson, 1970; Maderson et al., 1998; Bonfitto et al., 2022, 2023; Dujsebaieva et al., 2021; Griffing et al., 2021), friction is smoothened in serpentiform sliders that utilize mainly ventral and caudal scales for gripping onto the substrate and pushing the anterior part of their body forward (Spinner et al., 2015). The smooth surface and compaction of scales determines formation of a streamline surface that facilitates oscillatory serpentine movements generating frictional anisotropy forces for the

forward movement but also for digging. Ventral scales of some snakes, although possessing lower frictional resistance than lateral or dorsal scales, however produce forces that favor the direction of the forward movement of these reptiles, a property called "frictional anisotropy" (Berthe et al., 2009; Klein and Gorb, 2014).

The above considerations explain the bare or however smooth Oberhautchen surface of the scale in the slow worm, a characteristic that tends to reduce friction. The few studies on microornamentation in scincids (Canei and Nonclercq, 2021) and anguids (Spinner et al., 2015) have revealed that the Oberhautchen surface is smooth but that the posterior perimeter of Oberhautchen cells present similar denticles as those here observed, indicated as microridges in lizards or "echinous" processes in snakes (Price, 1980; Price and Kelly, 1982). The only regions where microridges are present in *A. fragilis* are in the posterior ventral scales of the trunk and in ventral caudal scales, a mean that facilitate gripping to the substrate for locomotion in this species, indicated as "slide-pushing" (Spinner et al., 2015). Similar aspects were noted for skinks such as *Scincus scincus* and *Eumeces schneideri,* that also revealed an epidermal surface made of irregular-shaped Oberhautchen cells with a smooth surface, although the microridges were also observed in the dorsal scales of the trunk (Canei and Nonclercq, 2021). These nanostructural similarities in fossorial serpentiform species support the hypothesis that the denticles favor the "slide-pushing" movement of this fossorial species. Variably densely distributed microridges are typical of snake scales where their number and size is correlated to different microhabitats adaptations (Gowers, 2003; Rhoca-Barbosa and e Silva, 2009). The presence of denticles or microridges in Oberhautchen cells of ventral and some lateral scales of the posterior trunk and tail region likely increases the gripping of this areas on the substrate. This firm but temporarily contact generates forces which serve for the forward movement of legless lizards that use the posterior ventral scales for holding on the substrate while the anterior part of the body undulates forward (Spinner et al., 2015).

Scales of *A. fragilis* lack of keels, differently from those present in the anguid *Pseudopus apodus* (Spinner et al., 2015), structural prominences retained to delay wearing and favor the undulating lateral movement. Wearing of the scale perimeter is frequent detect in *A. fragilis*, likely derived from the continuous contact and consequent scale abrasion from the ground during slithering (Klein and Gorb, 2014).

4.3. Sensory organs

The type of sensory organs identified in *A. fragilis* are of the circular flat type, adapted for a fossorial activity that would otherwise creates abrasion problems for spinulated sensilli with long setae as in geckos, agamids and some iguanids (Ananieva et al., 1991; Dujesebayeva et al., 2021;

Bonfitto et al., 2022, 2023). Also, the localization of sensilli of discoid or bouton-like shape on the head region in the slow worm resembles similar sensory organs detected in other species of lizards and snakes (Jackson, 1977; Matveyeva and Ananjeva, 1995; Harvey and Gutberlet, 1995; Sherbrooke and Nagle, 1996; Fig. 7). The histological analysis has revealed that these smooth receptors are formed by thinning of beta- and alpha-layers with respect to the surrounding regions of scales, under which specialized epidermal cells with numerous terminal sensory nerves are localized (Sherbrooke and Nagle, 1996). The exclusive localization of these flat or lenticular sensilli in the most apical scales of the head suggests that the slow worm can sense the environment and maybe also determine the ground resistance when the lizard is digging, acting as pressure receptors that allow orienting the reptile toward softer substrates. This hypothesis should however be evaluated in future studies.

Acknowledgments: the present work was supported by Canziani Bequest Fund, University of Bologna (grant number A.31.CANZELSEW), Bologna, (A. Bonfitto), and from Comparative Histolab Padova (L. Alibardi). We declare no conflict of interest in our manuscript.

REFERENCES

Alibardi, L. (1999). Keratohyalin-like granules in embryonic and regenerating epidermis of lizards and *Sphenodon punctatus* (Reptilia, Lepidosauria). *Amphibia-Reptilia 20*, 11-23.

Alibardi, L. (2014a). Comparative immunolocalization of Keratin-associated beta-proteins (Beta-keratins) supports a new explanation for the cyclical process of keratinocyte differentiation in lizard epidermis. *Acta Zoologica 95*, 32-43.

Alibardi, L. (2014b). Immunoreactivity of the pre-core box antibody shows that most glycine-rich beta proteins accumulate in lepidosaurian beta-layer and in the corneous layer of crocodilian and turtle epidermis. *Micron 57*, 31-40.

Alibardi, L., & Toni M. (2006). Cytochemical, biochemical and molecular aspects of the process of keratinization in the epidermis of reptilian scales. *Progress in Histochemistry and Cytochemistry 40*, 73-134.

Ananjeva, N.B., Dilmuchamedov, M.E., & Matveyeva, T.N. (1991). The skin sense organs of some iguanian lizards. *Journal of Herpethology 25*, 186-199.

Arnold, E.N. (2002). History and function of scale microornamentation in lacertid lizards. *Journal of Morphology 252*, 145-169.

Berthe, R.A., Westhoff, G., Bleckmann, H., & Gorb, S.N. (2009). Surface structure and frictional properties of the skin of the Amazon tree boa *Corallus hortulanus* (Squamata, Boidae). *Journal of Comparative Physiology 195*, 311-318.

Bonfitto, A., Bussinello, D., & Alibardi, L. (2022). Electron microscopic analysis in the gecko *Lygodactylus* reveals variations in micro-ornamentation and sensory organs distribution in the epidermis that indicates regional functions. *Anatomical Record* 306, 1990-2014.

Bonfitto, A., Randi, R., Magnani, M., & Alibardi, L. (2023). Micro-ornamentation patterns in different areas of the epidermis in the gecko *Tarentola mauritanica* reflect variations in the accumulation of corneous material in Oberhautchen cells. *Protoplasma* doi.org/10.1007/s00709-023-01860-8.

Canei, J., & Nonclercq, D. (2021). Morphological study of the integument and corporal skeletal muscles of two psammophilus members of Scincidae (*Scincus scincus* and *Eumeces schneideri*). *Journal of Morphology* 282, 230-246.

Cherepanov, G.O., Gordeev, D., Melnikov, D.A., & Ananjeva, N.B. (2023). Osteoderm development during regeneration process in *Eurylepis taeniolata* Blyth, 1854 (Scincidae, Sauria, Squamata). *Journal of Developmental Biology 11*, 22.

Dujsebayeva, T., Ananjeva, N., & Bauer, A.M. (2021). Scale microstructures of pygopodid lizards (Gekkota: Pygopodidae): phylogenetic stability and ecological plasticity. *Russian Journal of Herpethology 28*, 291-308.

Gower, D.J. (2003). Scale microornamentation of uropeltid snakes. *Journal of Morphology 258*, 249-268.

Griffing, A.H., Sanger, T.J., Epperlein, L., Bauer, A.M., Cobos, A., Higham, T.E., Naylor, & E., Gamble, T. (2021). And thereby hangs a tail: morphology, developmental patterns and biomechanics of the adhesive tail of crested geckos (*Correlophus ciliates*). *Proceedings of the Royal Society B 288*, 20210650.

Harvey, M.B., & Gutberlet, R.L. (1995). Microstructure, evolution and ontogeny of scale surfaces in cordilyd and gerrosaurid lizards. *Journal of Morphology 226*, 121-136.

Irish, F., Williams, E., & Seiling, E. (1988). Scanning electron microscopy of changes in epidermal structure occurring during the shedding cycle in squamate reptiles. *Journal of Morphology 197*, 105-126.

Jackson, M.K. (1977). Histology and distribution of cutaneous touch corpuscles in some Leptotyphlopid and Colubrid snakes (Reptilia, Serpentes). *Journal of Herpethology 11*, 7-15.

Klein MC.G., & Gorb, S.N. (2014). Ultrastructure and wear patterns of the ventral epidermis of four snake species (Squamata, Serpentes). *Zoology 117*, 295-314.

Maderson, P.F.A. (1970). Lizard glands and lizard hands: Models for evolutionary study. *Forma Functio 3*, 179-204.

Maderson, P.F.A., Rabinowitz, T., Tandler, B., & Alibardi, L. (1998). Ultrastructural contributions to an understanding of the cellular mechanisms involved in lizard skin shedding with comments on the function and evolution of a unique lepidosaurian phenomenon. *Journal of Morphology 236*, 1-24.

Matveyeva, T.N., & Ananjeva, N.B. (1995). The distribution and number of the skin sense organs of agamids, iguanid and gekkonid lizards. *Journal of Zoology 235*, 253-268.

Mazzi, V. (1977). Manuale di tecniche istologiche e istochimiche. Piccin Ed, Padova

Pough, F.H., Andrews, R.M., Cadle, J.E., Crump, M.L., Savitzky, A.H., & Wells, K.D. (2001). *Herpethology*, 2nd Edition, Prentice Hall, Upper Saddle River, New Jesrey, USA.

Price, R.M. (1982). Dorsal snake scale microdermatoglyphics: ecological indicator or taxonomic tool ? *Journal of Herpethology 16*, 294-306.

Price, R.M., & Kelly, P. (1989). Microdermatoglyphics: basal patterns and transitional zones. *Journal of Herpethology 23*, 244-261.

Ruibal, R. (1968). The ultrastructure of the surface of lizard scales. *Copeia 4*, 698-703.

Rhoca-Barbosa, O., & Morales e Silva, R.B. (2009). Analysis of the microstructure of Xenodontidae snake scales associated with differential habitat occupation strategies. *Brazilian Journal of Biology 69*, 919-923.

Scala, C., Cenacchi, G., Ferrari, C., Pasquinelli, G., Preda, P., & Manara, G.C. (1992). A new acrylic resin formulation: a useful tool for histological, ultrastructural, and immunocytochemical investigations. *Journal of Histochemistry and Cytochemistry 40*, 1799-1804.

Sheerbrooke, W.C., & Nagle, R.B. (1996). A dorsal intraepidermal mechanoreceptor in horned lizard (*Phrynosoma*; Phrynosomatidae; Reptilia). *Journal of Morphology 228*, 145-154.

Shortbridge, A. (2023). *Anguis fragilis*, Slow worm (http://animaldiversity.org/accounts/Anguis_fragilis).

Smith, H., Duvall, D.D., Graves, B.M., Jones, R.E., & Vhiszar, D. (1982). The function of squamate epidermatoglyphics, *Philadelphia Herpethological Society 30*, 1-4.

Spinner, M., Bleckmann, H., & Westhoff, G. (2015). Morphology and frictional properties of *Pseudopus apodus* (Anguidae, Reptilia). *Zoology 118*, 171-175.

Staudt. K., Saxe, F.P.M., Schmied, R.S., Bohme, W., & Baumgartner, W. (2012). Comparative investigations of the snadfish's β-keratin (Reptilia: Scincidae : *Scincus scincus*). Part 1: surface and molecular examinations. *Journal of Biomimetics and Biometarial Tissues and Engineering 15*, 1-16.

Stewart, G.R., & Daniel, R.S. (1973). Scanning electron microscopy from different body regions of three lizard species. *Journal of Morphology 139*, 377-388.

Swadzba, E., & Rupik, V. (2010). Ultrastructural studies of epidermis keratinization in grass snake embryos *Natrix natrix* L. (Lepidosauria, Serpentes) during late embryogenesis. *Zoology 113*, 339–360.

Vickaryous, M., & Sire, Y.S. (2009). The integumentary skeleton of tetrapods: origin, evolution, and development. *Journal of Anatomy 214*, 441-464.

Williams, C., Kirby, A., Marghoub, A., Kever, L., Ostashevskaya-Gohstand, S., Bertazzo, S., Moazen, M., Abzhanov, A., Herrel, A., Evans, S.E., & Vickaryous, M. (2022). A review of the osteoderms of lizards (Reptilia: Squamata). *Biological Review 97*, 1-19.

Zylberberg, L., Castanet, J. (1985). New data on the structure and the growth of the osteoderms in the reptile *Anguis fragilis* (Anguidae, Squamata). *Journal of Morphology 186*, 327-342.

Figure captions

Fig. 1. Histology of tail scales of *A. fragilis.* Toluidine blue stain (**A, B**) and Von Kossa-Blu tol stain (**C**). **A**, scales showing the epidermis (e), the corneous beta-layer (arrow), the hinge region (h), and the large osteoderm in the dermis (ost). Bar, 20 μm. **B**, detail focusing on the dome-like structures of most acellular osteodermin, surrounded by flat osteoblasts of the periosteum (arrows). Arrowheads indicate ostecytes within osteoderms. The asterisks indicate that the beta-layer is not included in this image (artifactually detached during sectioning). Bar, 10 μm. **C**, dark-stained, irregular-shaped osteoderms as revealed from the von Kossa reaction. Bar, 20 μm. **Legends**: de, dermis; e, epidermis; osd, osteodermin; ost, osteoderm; dashes undeline the epidermis.

Fig. 2. Histology (**A**) and immunofluorescence for CBPs (**B-E**) of tails scales in *A. fragilis*. **A**, detail by the tip of a scale with a thick beta-layer (arrow). Toluidine blue stain. Bar, 10 μm. **B**, immunolabeled beta-layer (green fluorescence from FITC) using the beta-1 antibody (β1). Dashes outline the scale shape. Bar, 10 μm. **C**, TRITC-immunolabeled beta-layers (arrows, red) in two extremely overlapped scales using the preCB antibody. Bar, 10 μm. **D**, detail of the thick

immunoflorescent beta-layer (arrow) of the central part of a scale. Bar, 10 µm. **E**, immunonegative control section (the arrow indicates the beta-layer). Bar, 20 µm. Legends: i, inner scale surface; t, tip; dashes undeline the epidermis in **C, D** and **E**.

Fig. 3. Scanning electron microscopic view of dorsal head scales in *A. fragilis*. **A**, general view (arrow indicates the apex) featuring the different shape and size of scales (ey, eyes orbit) Bar, 800 µm. **B**, detail showing the scale boundaries (arrows) and small disk-like (bouton-like) sensilli (arrowheads). Bar, 300 µm. **C**, close-up to front scales (maxillar) with numerous disk-like sensilli (arrwheads). Arrows indicate areas of likely scale deformations. Bar, 500 µm. **D**, detail of apical scales featuring the overlapped wore margin (arrow) of an anterior scales with the following one, and three disk-sensilli (arrowhead). Bar, 80 µm. **E**, close-up to a disk-sensilla. Arrowheads point to superficial cell boundaries (Oberhautchen cells). Bar, 25 µm. **F**, higher view showing the smooth Oberhautchen cell surface (ob) forming a tile-like pattern. Bar, 10 µm.

Fig. 4. SEM view of head gular scales (**A, B**) and trunk scales (**C-F**). Rostral direction in all figures is on the left. **A**, ventral view (gular) of scales shapes. The arrow points the apical (rostral) direction. Bar, 1 mm. **B**, detail of three overlapping scales located near the apex of the head (throat) with sensilla (arrowhead) and signs of wearing along their overlapped borders (arrow). Bar, 100 □m. **C**, panoramic image of the trunk showing the uniform shape of trapezoid and overlapped dorsal scales. Bar, 1 mm. **D**, overlapped scales of a lateral (flank) region. Bar, 600 µm. **E**, detail of lateral trunk, extremely overlapped scales with wore borders (arrows). Bar, 200 µm. **F**, higher magnification view of flank scales evidencing wearing (arrows) and the tile-like pattern of Oberhautchen cells. Bar, 100 µm. The inset (Bar, 15 µm) detail on the wore border (arrowhead) and showing the irregular outline Oberhautchen cells boundaries.

Fig. 5. SEM images of ventral trunk scales. **A**, detail of two scales showing Oberhautchen cells forming a tile-like surface. Arrows on wore/damaged border. Bar, 50 µm. **B**, close-up to show the irregualr perimeter of Oberhautchen cells (ob) forming an interlocked surface. Bar, 10 µm. **C**, shape variation of Oberhautcchen cells with numerous "denticles" on the posterior (caudal) side (arrows) that lightly overlap the following cell. Bar, 5 µm. The inset (Bar, 2 µm) magnifies the denticles.

Fig. 6. SEM (**A, B**) and TEM (**C-H**) images of *A. fragilis* surface of the epidermis. **A**, general distribution of ventral tail scales. Bar, 1 µm. The inset (Bar, 1 µm) shows a high magnification of the overlapped and denticulated border of a Oberhautchen cells with the next cell. **B**, close-up to

overlapped tail scales with wore borders (arrows). Bar, 150 μm. **C**, slanted Oberhautchen surface on the dorsal scale surface. Arrows point to the denser Oberhautchen. Bar, 5 μm. **D**, thin slanted Oberhautchen (arrow) on the inner scale surface. Bar, 5 μm. **E**, Oberhautchen in the hinge region (interscale) with thick mesos-layer. Bar, 1 μm. **F**, higher magnification on the transition between merged Oberhautchen and beta.layer. Arrowhead indicate the denser superficial thickening of the Oberhautchen. Arrows point to several junctional remnants. Bar, 100 nm. **G**, high magnification detailing the aspect of cell junctional remnants (arrows) with the electron pale beta-layer. Bar, 100 nm. **H**, lowermost part of the beta-layer transiting into the mesos-layer. The asterisks indicate an artifactual space among mesos cells formed during sectioning. Bar, 200 nm. The inset (Bar, 200 nm) details on an intracellular pale and granulated material (arrow) present within a mesos cell.. **Legends**: β, beta-layer; m, mesos cells; me, melanosomes; ob, Oberhautchen.

Fig. 7. Schematic drawing of head scales with sensilli (red dots) observed in dorsal (A), lateral (B) and ventral (C) projection. Different colors refer to the scales bearing the sensilli, as classified on the color list.

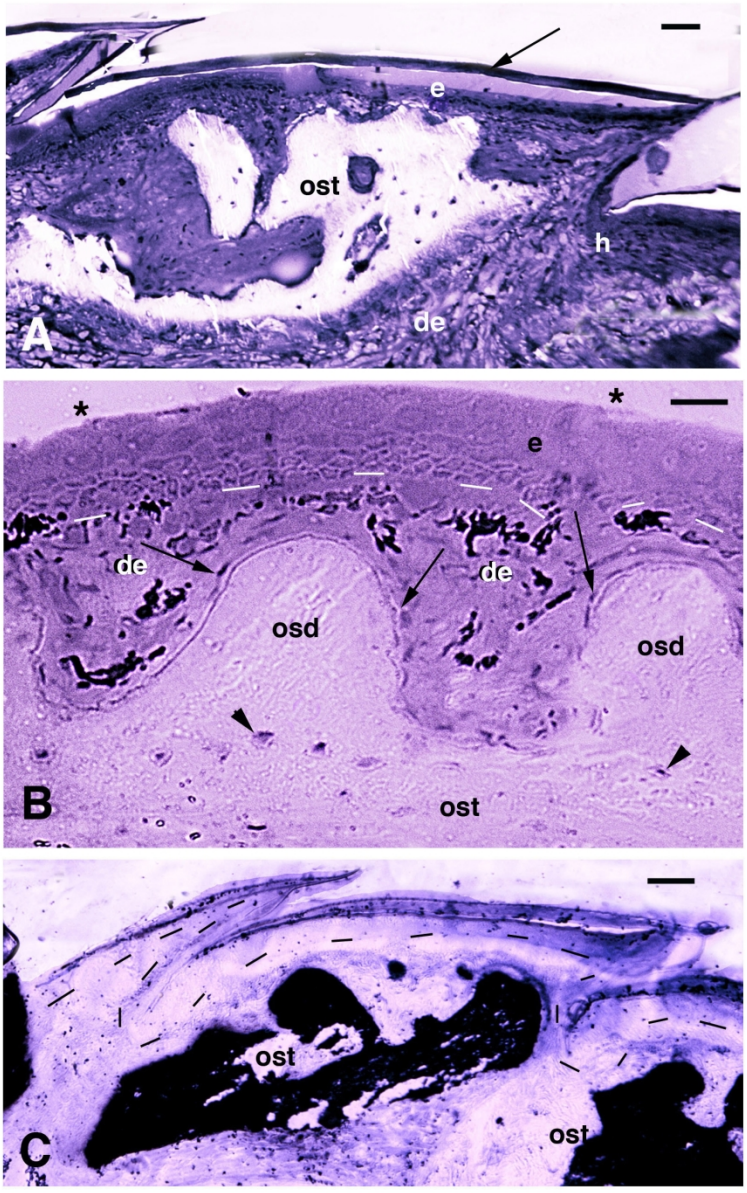

Fig. 1. Histology of tail scales of A. fragilis. Toluidine blue stain (A, B) and Von Kossa-Blu tol stain (C). A, scales showing the epidermis (e), the corneous beta-layer (arrow), the hinge region (h), and the large osteoderm in the dermis (ost). Bar, 20 μm. B, detail focusing on the dome-like structures of most acellular osteodermin, surrounded by flat osteoblasts of the periosteum (arrows). Arrowheads indicate ostecytes within osteoderms. The asterisks indicate that the beta-layer is not included in this image (artifactually detached during sectioning). Bar, 10 μm. C, dark-stained, irregular-shaped osteoderms as revealed from the von Kossa reaction. Bar, 20 μm. Legends: de, dermis; e, epidermis; osd, osteodermin; ost, osteoderm; dashes undeline the epidermis.

140x219mm (300 x 300 DPI)

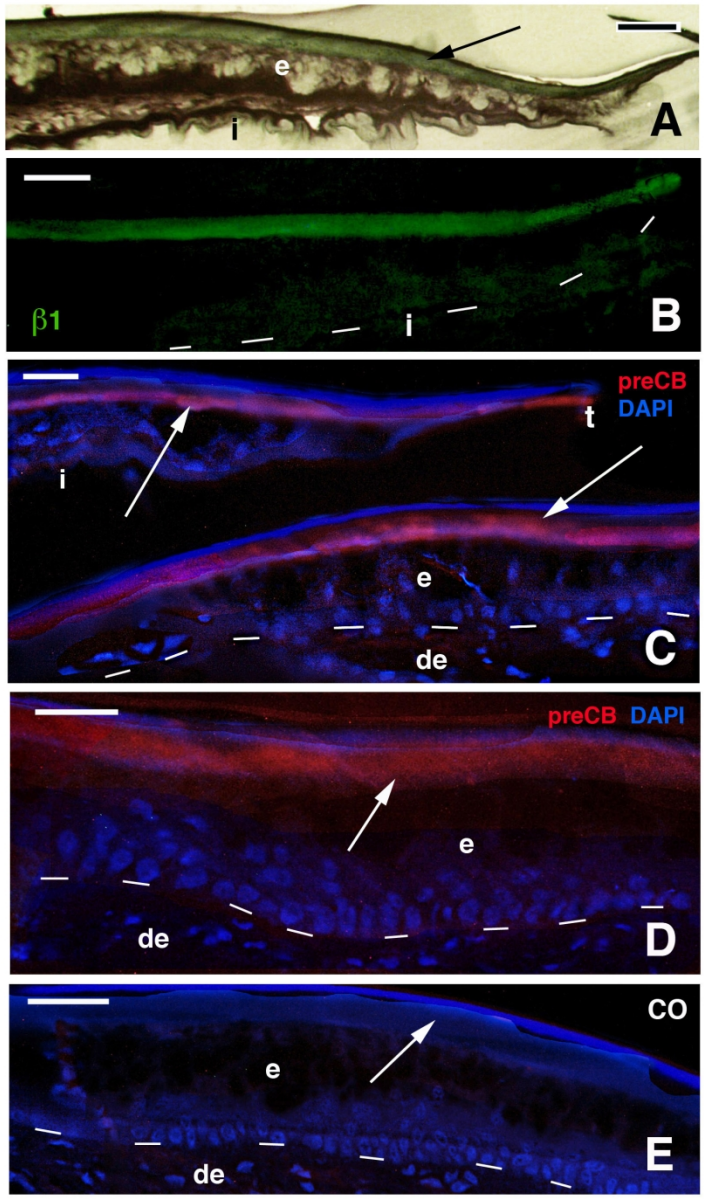

Fig. 2. Histology (A) and immunofluorescence for CBPs (B-E) of tails scales in A. fragilis. A, detail by the tip of a scale with a thick beta-layer (arrow). Toluidine blue stain. Bar, 10 μm. B, immunolabeled beta-layer (green fluorescence from FITC) using the beta-1 antibody (β1). Dashes outline the scale shape. Bar, 10 μm. C, TRITC-immunolabeled beta-layers (arrows, red) in two extremely overlapped scales using the preCB antibody. Bar, 10 μm. D, detail of the thick immunoflorescent beta-layer (arrow) of the central part of a scale. Bar, 10 μm. E, immunonegative control section (the arrow indicates the beta-layer). Bar, 20 μm. Legends: i, inner scale surface; t, tip; dashes undeline the epidermis in C, D and E.

131x219mm (300 x 300 DPI)

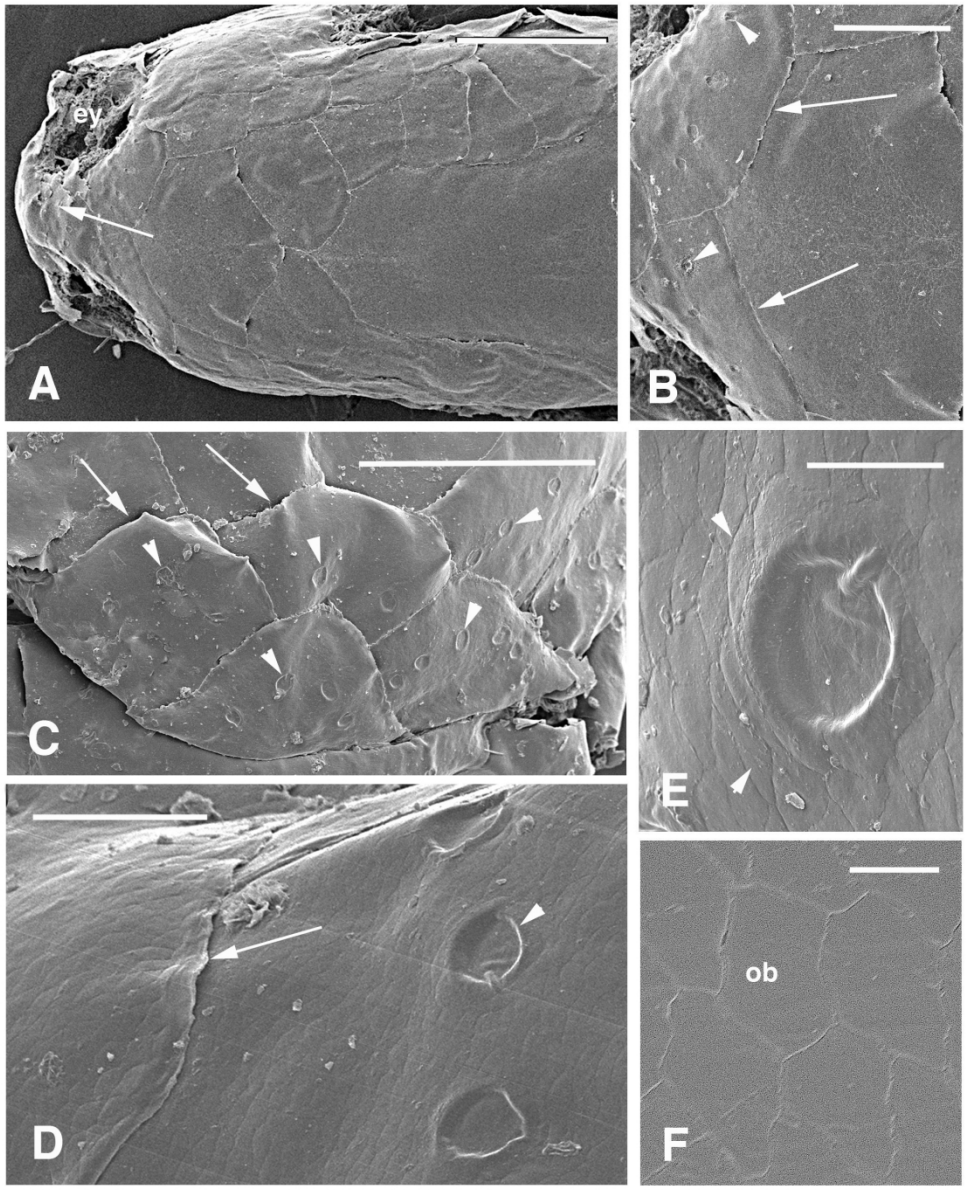

Fig. 3. Scanning electron microscopic view of dorsal head scales in A. fragilis. A, general view (arrow indicates the apex) featuring the different shape and size of scales (ey, eyes orbit) Bar, 800 µm. B, detail showing the scale boundaries (arrows) and small disk-like (bouton-like) sensilli (arrowheads). Bar, 300 µm. C, close-up to front scales (maxillar) with numerous disk-like sensilli (arrwheads). Arrows indicate areas of likely scale deformations. Bar, 500 µm. D, detail of apical scales featuring the overlapped wore margin (arrow) of an anterior scales with the following one, and three disk-sensilli (arrowhead). Bar, 80 µm. E, close-up to a disk-sensilla. Arrowheads point to superficial cell boundaries (Oberhautchen cells). Bar, 25 µm. F, higher view showing the smooth Oberhautchen cell surface (ob) forming a tile-like pattern. Bar, 10 µm.

180x219mm (300 x 300 DPI)

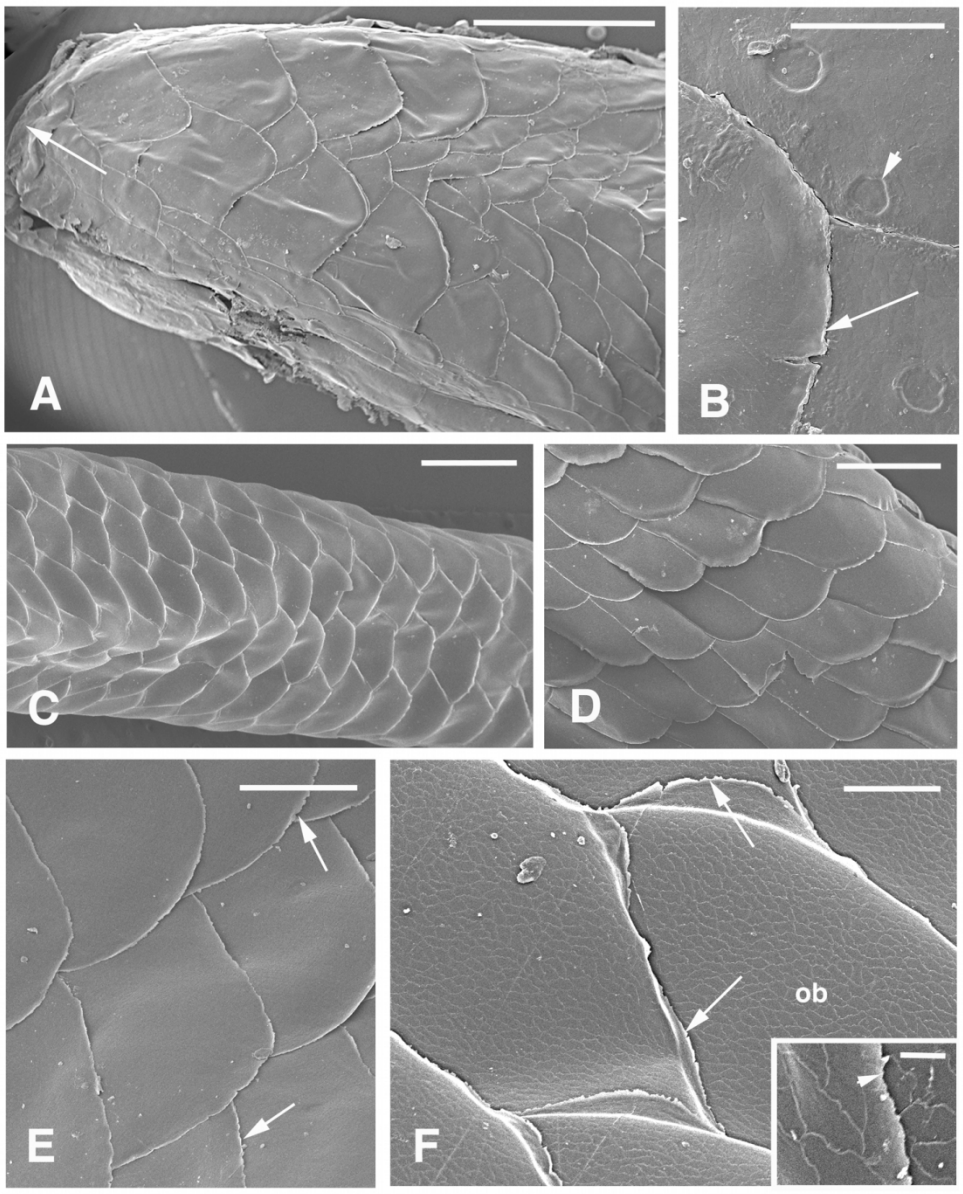

Fig. 4. SEM view of head gular scales (A, B) and trunk scales (C-F). Rostral direction in all figures is on the left. A, ventral view (gular) of scales shapes. The arrow points the apical (rostral) direction. Bar, 1 mm. B, detail of three overlapping scales located near the apex of the head (throat) with sensilla (arrowhead) and signs of wearing along their overlapped borders (arrow). Bar, 100 □m. C, panoramic image of the trunk showing the uniform shape of trapezoid and overlapped dorsal scales. Bar, 1 mm. D, overlapped scales of a lateral (flank) region. Bar, 600 µm. E, detail of lateral trunk, extremely overlapped scales with wore borders (arrows). Bar, 200 µm. F, higher magnification view of flank scales evidencing wearing (arrows) and the tile-like pattern of Oberhautchen cells. Bar, 100 µm. The inset (Bar, 15 µm) detail on the wore border (arrowhead) and showing the irregular outline Oberhautchen cells boundaries.

127x155mm (300 x 300 DPI)

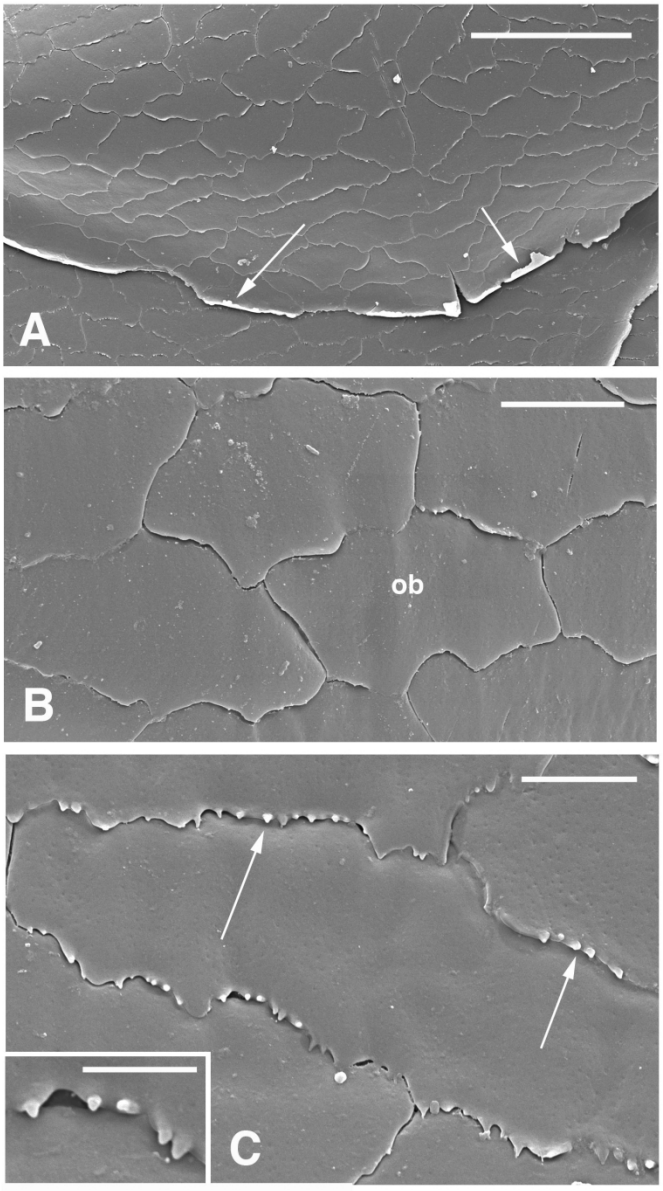

Fig. 5. SEM images of ventral trunk scales. A, detail of two scales showing Oberhautchen cells forming a tile-like surface. Arrows on wore/damaged border. Bar, 50 µm. B, close-up to show the irregualr perimeter of Oberhautchen cells (ob) forming an interlocked surface. Bar, 10 µm. C, shape variation of Oberhautcchen cells with numerous "denticles" on the posterior (caudal) side (arrows) that lightly overlap the following cell. Bar, 5 µm. The inset (Bar, 2 µm) magnifies the denticles.

123x219mm (300 x 300 DPI)

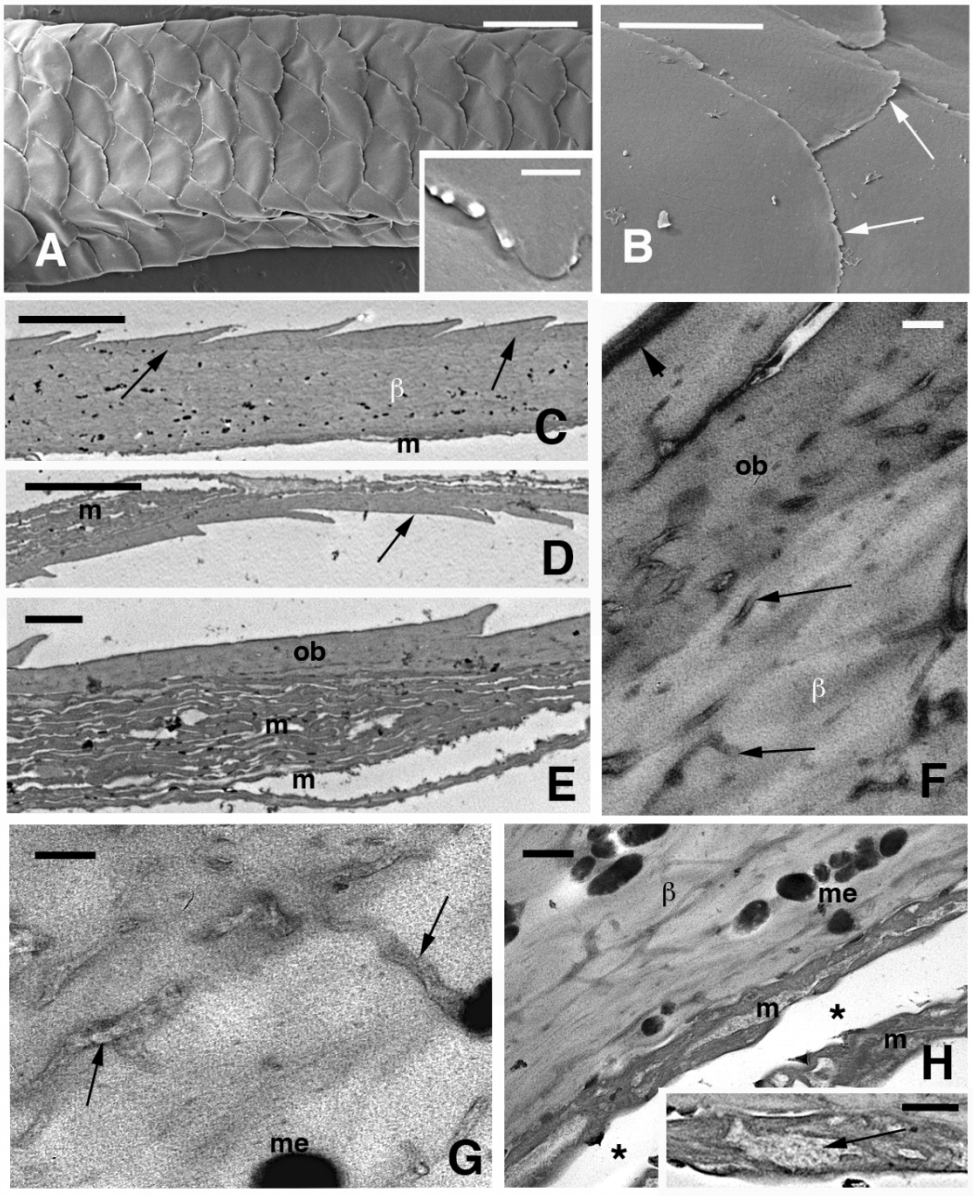

Fig. 6. SEM (A, B) and TEM (C-H) images of A. fragilis surface of the epidermis. A, general distribution of ventral tail scales. Bar, 1 μm. The inset (Bar, 1 μm) shows a high magnification of the overlapped and denticulated border of a Oberhautchen cells with the next cell. B, close-up to overlapped tail scales with wore borders (arrows). Bar, 150 μm. C, slanted Oberhautchen surface on the dorsal scale surface. Arrows point to the denser Oberhautchen. Bar, 5 μm. D, thin slanted Oberhautchen (arrow) on the inner scale surface. Bar, 5 μm. E, Oberhautchen in the hinge region (interscale) with thick mesos-layer. Bar, 1 μm. F, higher magnification on the transition between merged Oberhautchen and beta.layer. Arrowhead indicate the denser superficial thickening of the Oberhautchen. Arrows point to several junctional remnants. Bar, 100 nm. G, high magnification detailing the aspect of cell junctional remnants (arrows) with the electron pale beta-layer. Bar, 100 nm. H, lowermost part of the beta-layer transiting into the mesos-layer. The asterisks indicate an artifactual space among mesos cells formed during sectioning. Bar, 200 nm. The inset (Bar, 200 nm) details on an intracellular pale and granulated material (arrow) present within a mesos cell.. Legends: β, beta-layer; m, mesos cells; me, melanosomes; ob, Oberhautchen.

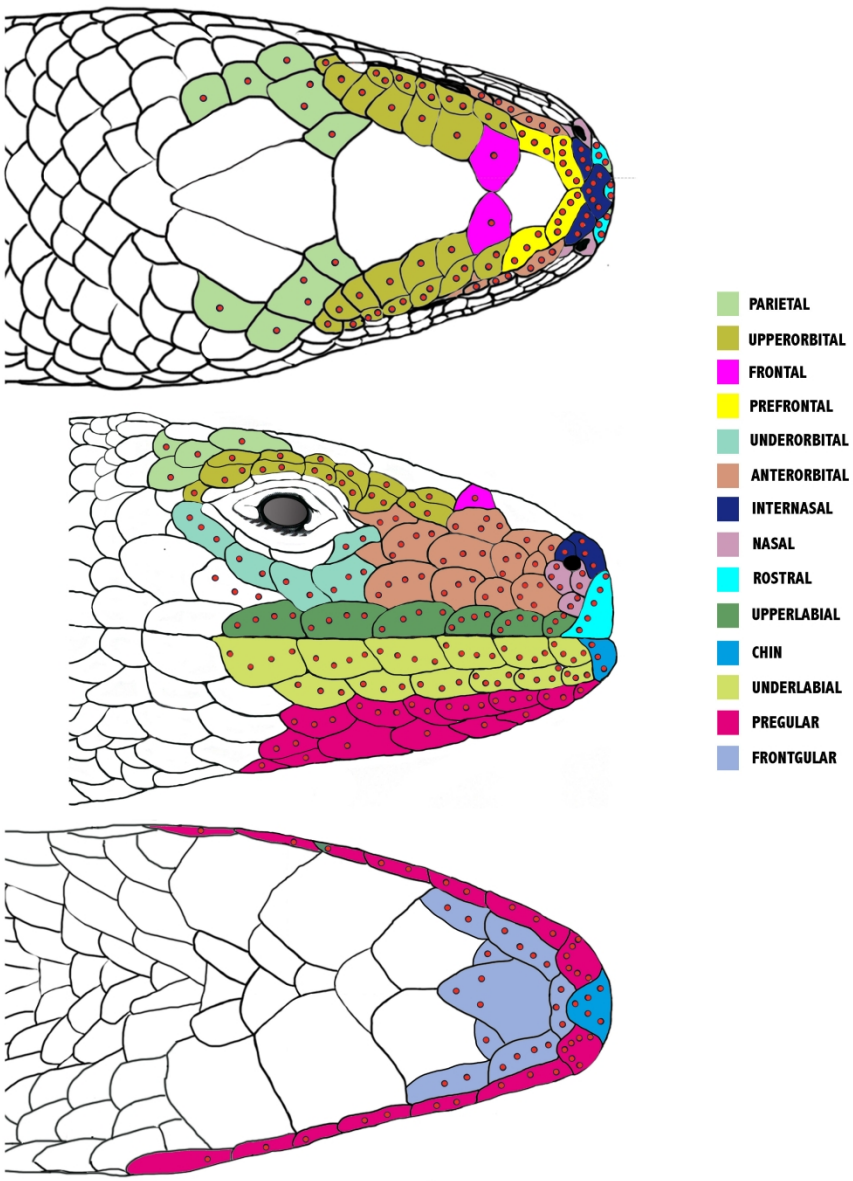

Fig. 7. Schematic drawing of head scales with sensilli (red dots) observed in dorsal (A), lateral (B) and ventral (C) projection. Different colors refer to the scales bearing the sensilli, as classified on the color list.

275x345mm (299 x 299 DPI)